IOP Publishing | Astro Ltd Laser Physics Letters
Laser Phys. Lett. **21** (2024) 075101 (15pp) https://doi.org/10.1088/1612-202X/ad51e2

Letter

Design and analysis of the C_6H_6-filled circular photonic crystal fiber with ultra-flat dispersion for broadband supercontinuum generation with peak power of 130 W and 250 W

Duc Hoang Trong[1], Lanh Chu Van[2] and Thuy Nguyen Thi[1,*]

[1] University of Education, Hue University, 34 Le Loi, Hue City, Vietnam
[2] Department of Physics, Vinh University, 182 Le Duan, Vinh City, Vietnam

E-mail: ntthuy@hueuni.edu.vn

Received 18 February 2024
Accepted for publication 27 May 2024
Published 10 June 2024

Abstract

This article introduces a new model of a circular silica-based photonic crystal fiber with a hollow core filled with C_6H_6. The difference in the air hole size and the distance between them in the first ring around the core has a profound effect on the dispersion, leading to ultra-flat dispersion with values as low as ± 0.996 ps nm^{-1} · km in wavelength range 0.74 μm. The high nonlinear coefficient of several 1000 W^{-1} · km^{-1} and the low confinement loss of a few tens of dB m^{-1} suggest proposing three fibers with dispersion and nonlinear properties suitable for broadband supercontinuum generation at low peak power. The influence of peak power on the broadening of the supercontinuum spectrum is also investigated. Fibers with a flat all-normal dispersion profile provide a smooth spectrum with bandwidths of 1.215 and 1.626 μm at 30 dB with a peak power of 250 W. A fiber with an anomalous dispersion regime generates a supercontinuous spectrum, broadening to 3.868 μm in the mid-infrared region (2.467 μm bandwidth at 30 dB) under laser pulse excitation with 130 W peak power. Our results provide further insights into the generation of broadband mid-infrared supercontinuum using liquid-core silica-fibers, which have great potential for applications in the fields of optical communications and optical sensing.

Keywords: liquid-core PCF, C_6H_6 infiltration, mid-infrared supercontinuum, low peak power, ultra-flat dispersion

1. Introduction

The phenomenon of supercontinuum generation (SCG) that produces broadband, spatially coherent, and high-brightness light sources from extremely short pulses, has consistently served as an endless source of inspiration for fiber optic researchers. This is due to its diverse applications in many fields of science and technology, such as spectroscopy, optical communications, biomedical imaging, sensors [1–4], etc. The key challenges in enhancing SCG efficiency related to the spectral width and flatness over a wide wavelength band. This requires the flat dispersion and suitable nonlinear characteristics of the photonic crystal fibers (PCFs). The flexibility in PCF design and the selection of an optimal pump location can effectively meet these requirements. Recently, various

* Author to whom any correspondence should be addressed.

methods to control PCF dispersion have been developed including the use of highly nonlinear substrates such as glass chalcogenides and semiconductor materials [5, 6], tapered fibers [7] or fibers with diverse geometries [8–10]. Among these silica-PCF is more popular because the characteristics of silica (SiO_2) material make the fiber production process more convenient. This increases the possibility of applying SCG in practice. However, the major limitation is the fact that the SCG spectrum using silica-PCF is extends beyond the mid-infrared application limit due to the multiphonon transmission edge [11]. To overcome this problem, many studies have been conducted to identify the most effective method for SCG generation. PCFs with new models are investigated through theoretical numerical simulation and experiment, focusing on changing a number of structural parameters, including cross-section, fiber core, air hole size in the cladding [8, 12–14] or highly nonlinear fluid filling the hollow core [15–23]. As a result, low-value, ultra-flat dispersion [9, 18], high nonlinearity [22, 23], and low attenuation [20, 21] have been achieved broadening the SCG spectrum in the near-infrared and mid-infrared regions. Although concerns exist regarding the complex fiber structure, the rapid development of fiber optic technology today renders silica-PCFs feasible for fabrication [17, 24, 25].

Using PCF as a nonlinear medium for SC generation represents a major breakthrough that elevates the position of this field due to its flexible dispersion properties, including profile, flatness, value, slope, and zero dispersion wavelengths (ZDWs). These are important factors that determine the emergence of a series of related nonlinear effects and their interactions as femtosecond pulses undergo spectral broadening in the PCF core [26]. When the pulse propagates in the PCF under normal dispersion regime, self-phase modulation (SPM), optical wave breaking (OWB) and four-wave mixing (FWM) [27] are important effects contributing to the broadening of the spectrum. Notably, SCG performed in PCFs with all-normal dispersion often results in smooth, highly coherent spectra due to noise-induced effects such as modulation instability, stimulated Raman scattering (SRS), and collisions of many chaotic solitons can be suppressed [28]. This feature is very important in optical coherence tomography [29]. On the other hand, nonlinear effects within the framework of soliton dynamics govern the broadening of the SCG spectrum when the fiber is pumped in the anomalous dispersion regime, near the ZDW. The transformation of the input pulse into higher order solitons through soliton fission (SF) and SRS usually causes the spectrum to be noisy, but soliton self-frequency shift (SSFS) results in a red shift. Blue shift is often affected by blue-shifted dispersive waves (DWs). The SCG spectral features produced, whether the PCF-pumped fiber is in anomalous or normal dispersion regimes, have their own interesting applications. Besides, the characteristic parameters of the input pulse, such as duration, energy, and peak power, are also necessary parameters that contribute to improving SCG quality. Therefore, achieving broadband SCGs with low peak power has always been the goal of research groups.

Related to this issue, several works have reported experimental and numerical demonstrations of broadband SCG sources based on liquid-core silica-PCFs. Experimentally, liquid core PCFs can be fabricated using standard fabrication, stacking, and drawing processes [17, 30, 31]. Commonly used nonlinear liquids include toluene (C_7H_8) [9, 16, 23], nitrobenzene ($C_6H_5NO_2$) [21], benzene (C_6H_6) [13, 32], carbon tetrachloride (CCl_4) [17], tetrachlorethylene (C_2Cl_4) [33, 34], chloroform ($CHCl_3$) [20, 35], carbon disulfide (CS_2) [22], and ethanol (C_2H_5OH) [18]. Choosing a variety of the cladding geometries or introducing defects into the air hole rings are suitable ways to control the dispersion properties of PCFs. The typical parabolic flat-all-normal, anomalous dispersions were obtained, and even the ultra-flat dispersion [18], with low value over a wide wavelength range, was found. Furthermore, a quite high nonlinear coefficient, up to several 1000 W^{-1} km^{-1}, and low losses favoring SCG spectrum expansion have also been reported. However, there have been no publications mentioning achieving mid-infrared broadband SCG with very low power, lower than 300 W.

In the group of aromatic compounds, C_6H_6 has a higher nonlinear refractive index ($n_2 = (0.6 - 5)\times 10^{-19}$ m^2 W^{-1}) than SiO_2 ($n_2 = 2.79 \times 10^{-20}$ m^2 W^{-1}) [36] similar to C_7H_8 and $C_6H_5NO_2$. Furthermore, it has low loss in the wavelength region up to 14 μm [37], which prevents some frequency components from being attenuated when forming a supercontinuum along the fiber due to free soliton shifts, OWB, and SPM. Careful consideration is required for low-temperature applications involving C_6H_6, as its freezing point is 5.5 °C (similar to $C_6H_5NO_2$). To date, there have been few studies on SCG using C_6H_6-infiltrated hollow-core PCFs with geometries such as hexagonal, circular and square lattice, where the difference in air hole size in the cladding is exploited. The publication [32] obtained the widest SCG spectrum from 0.6 μm to 3.5 μm but with the peak power up to 22.2 kW for fiber with anomalous dispersion. For an all-normal dispersion fiber, the SCG bandwidth at 15 dB is 1.3 μm but the peak power is very high, up to 55 kW. When the air hole size in the first ring near the core is smaller than the others, the PCFs investigated in the works [13, 38, 39] show better SCG spectrum broadening [32] with much lower peak power, ranging from about 450 W to 790 W. However, the ultra-flat dispersion with low value across a wide wavelength range, which is so beneficial for SCG spectral broadening, has not yet been found.

PCFs with circular lattice also evince the potential to flexibly control the PCF to achieve ultra-flat, near-zero dispersion, which is the target for broadband SCGs with low peak power [40–41]. The circular lattice with high geometric symmetry can effectively confine the electromagnetic field in the core, enhancing the nonlinearity of the fiber. Furthermore, PCFs with circular lattices also expose good applicability in spectroscopy, pulse compression, dense wavelength division multiplexing-based telecommunication systems, and sensing applications [40, 42]. In this work, we verify, for the first time, the potential to generate the broadband mid-infrared SCGs with peak powers lower than 300 W using C_6H_6-filled core circular lattice PCFs. The dispersion and nonlinear properties are optimized by eliminating the periodicity of air holes in the cladding. The flat all-normal and anomalous dispersions with

small values at the suitable pump wavelengths were found. In particular, the optimal PCF has ultra-flat, near-zero all-normal dispersion, with $\Delta D = \pm\ 0.996$ ps nm^{-1} · km in wavelength range of 0.74 μm, providing a broadband SCG spectrum at 30 dB of 1.626 μm with low peak power of 250 W. With a high nonlinearity of 2795.503 W^{-1} · km^{-1} and loss as low as 67.996 dB m^{-1}, PCF exhibits flat anomalous dispersion, emitting a broadband mid-infrared SCG of 2.467 μm at 30 dB with a very low peak power of 130 W. The mechanisms involved in soliton dynamics and SPM are analyzed in detail for each case. In connection with our previous publications, these results continue to provide new insights into the potential of liquid core PCFs in mid-infrared, broadband, and low peak power SCG research.

2. PCFs design and optical properties computation

2.1. PCFs design

Figure 1(a) depicts the cross-sections of circular lattice PCFs with C_6H_6 infiltration. The structure of SiO_2-based PCFs consists of two regions including cladding and core. Eight rings of air holes are arranged in a circular pattern surrounding the core in the cladding, which makes the structure of the PCF more symmetrical and simpler for fabrication. The distance between the air holes (Λ) is different from the distance Λ_1 from the center of the core to the air hole of the first ring ($\Lambda_1 = 1.093\Lambda$). This ring has air holes with diameter d_1 smaller than d_2 of the others. To find the optimal structure, the dispersion and nonlinear properties of PCFs were investigated according to the change of d_1/Λ ratio from 0.3 to 0.65 with each step of 0.05 (Λ = 0.9 μm; 1.0 μm; 1.5 μm and 2.0 μm) while $d_2 = 0.95\Lambda$ is kept constant. The hollow core with diameter $D_c = 2\Lambda - 1.2d_1$ is filled with C_6H_6 to create a refractive index difference between the core and the cladding, thereby helping to best overcome the leakage of light from the core to the cladding region or between the air holes together. All air hole rings in the cladding play an important role in controlling the optical properties of the PCF, giving us the desired values. Introducing lattice defects into the first ring closest to the core strongly affects dispersion optimization, including shifting ZDW. The nonlinear properties, especially the confinement loss of the fundamental mode (or even at higher order modes), are strongly dominated by the remaining rings [43]. These are impressive suggestions for designing a circular C_6H_6-filled PCF by breaking the uniformity of the cladding region mentioned above. So, after careful selection of the structural parameters of the PCF, it is possible to achieve the desired dispersion properties. Such structures may raise concerns in fiber production, but the rapid development of optical fiber technology can solve such problems [10, 44].

The structure of circular PCFs with C_6H_6 infiltration is modeled using Lumerical Mode Solution software (LMS) [45]. Moreover, LMS also supports calculation of propagation coefficients as well as modes profiles related to the eigenvectors and eigenvalues. To successfully design the structure of PCFs, the coefficients in the Sellmeier and Cauchy

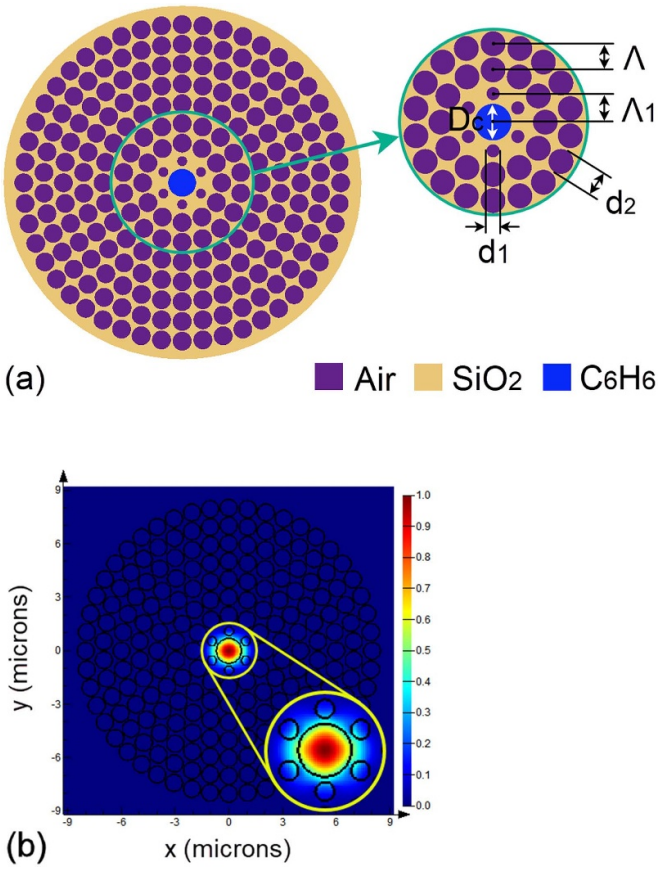

Figure 1. The cross-sectional views of C_6H_6-filled circular PCFs (a) and the light confinement in the core of PCF with $\Lambda = 1.0$ μm, $d_1/\Lambda = 0.5$ (b).

Table 1. Coefficients according to Sellmeier and Cauchy equation of SiO_2 and C_6H_6 refractive index.

A_1	0.696 1663	B_1	0.068 4043	C_1	2.170 184 597
A_2	0.407 9426	B_2	0.116 2414	C_2	0.000 593 99
A_3	0.897 4794	B_3	9.896 1610	C_3	0.023 034 64
				C_4	0.000 499 485
				C_5	0.000 178 796

equations [46, 47] for the refractive index of C_6H_6 and SiO_2 are declared in the LMS data system (with coefficients A_i, B_i, C_i given in table 1) and the structural parameters are calculated accordingly. The physical effects that occur when light propagates in PCF are analyzed through the numerical solution of Maxwell's wave equations using the full-vector finite-difference eigenmode (FDE) method. To compute the propagation coefficient β with high accuracy using the 'FDE solver' [48], the cross-section of the micrometer-sized PCF is divided into hundreds of thousands of very small rectangles called 'Yee's mesh'. Within each 'Yee's mesh', the optical properties change insignificantly. The cells across interfaces at points on the surface located between the two media are used for an index averaging technique. The minimum mesh step of 10^{-6} μm and 300 mesh cells without override regions

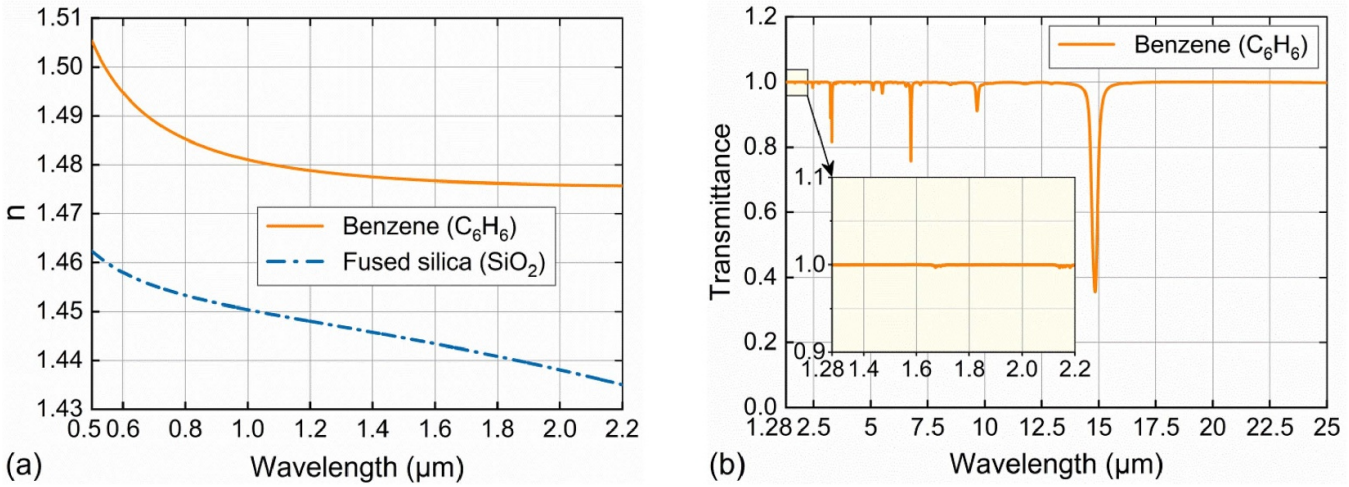

Figure 2. The real parts of the refractive index of C_6H_6 and SiO_2 is extrapolated using Sellmeier and Cauchy equation (a) and the transmittance spectrum of C_6H_6 [37] (b).

is set for PCFs. The optical properties of the PCFs investigated in the 0.6–2.2 μm wavelength range are compatible with reliable data in the LMS.

$$n^2_{SiO_2}(\lambda) = 1 + \frac{A_1\lambda^2}{\lambda^2 - B_1^2} + \frac{A_2\lambda^2}{\lambda^2 - B_2^2} + \frac{A_3\lambda^2}{\lambda^2 - B_3^2}, \quad (1)$$

$$n^2_{C_6H_6}(\lambda) = C_1 + C_2\lambda^2 + \frac{C_3}{\lambda^2} + \frac{C_4}{\lambda^4} + \frac{C_5}{\lambda^6}, \quad (2)$$

where λ is the excitation wavelength in micrometers, $n(\lambda)$ is the wavelength-dependent refractive index of materials.

The real part of the effective refractive index (n) of C_6H_6 and SiO_2 against the increase in wavelength is shown in figure 2(a). Furthermore, the n of C_6H_6 consistently surpasses the n of SiO_2, indicating that the refractive index of the core region is higher than the refractive index of the cladding region. Therefore, the process of adjusting the light propagation in the PCF is based on total internal reflection, similar to a conventional optical fiber. C_6H_6 demonstrates transparency over a wide wavelength, extending up to 25 μm, with some strong absorption peaks outside the 2.5 μm wavelength range, displayed in figure 2(b). This means that it has a large bulk attenuation in the wavelength region $\lambda > 2.5$ μm [37], which is mainly responsible for the loss of the proposed fibers in the long wavelength range. In the investigated wavelength range of 0.6–2.2 μm, C_6H_6 exhibits negligible loss.

2.2. Chromatic dispersion

The chromatic dispersion includes material dispersion and waveguide dispersion. It is essential for practical applications in dispersion compensation of nonlinear optics and optical communications. By modifying the geometric parameters of the PCFs, dispersion can be flexibly controlled and given the expected values. The waveguide dispersion is determined using [27]:

$$D = -\frac{\lambda}{c}\frac{\partial^2 \mathrm{Re}\left[n_{\mathrm{eff}}\right]}{\partial\lambda^2}, \quad (3)$$

where $\mathrm{Re}[n_{\mathrm{eff}}]$ is the real part of the effective index of the guided mode, λ and c are the wavelength and the speed of light in a vacuum, respectively.

2.3. Effective mode area

The effective mode area is an important parameter in the design of PCFs and the expansion of the SCG spectrum, that helps determine the degree of confinement of the mode field in the core. It can be calculated by [27]:

$$A_{\mathrm{eff}} = \frac{\left(\int_{-\infty}^{\infty}\int_{-\infty}^{\infty}|E|^2\mathrm{d}x\mathrm{d}y\right)^2}{\int_{-\infty}^{\infty}\int_{-\infty}^{\infty}|E|^4\mathrm{d}x\mathrm{d}y}, \quad (4)$$

where E is the amplitude of the transverse electric field propagating inside the PCF.

The nonlinear coefficient is inversely proportional to the effective mode area, it appears from the Kerr effect originating from the interaction of intense light with material. It is calculated according to the following formula [27]:

$$\gamma(\lambda) = 2\pi\frac{n_2}{\lambda A_{\mathrm{eff}}}, \quad (5)$$

with n_2 is the nonlinear refractive index for SiO_2.

3. Simulation results and discussion

In this section we focus solely on the analysis of the fundamental mode dispersion because higher order modes have a negligible effect on the spectral SCG broadening if the input pulse is short enough, less than 10 ps. To obtain broadband SCG, a fine-tuning of the dispersion profile is essential, and thus, the dispersion properties of all structures are investigated according to the change of ratio d_1/Λ and Λ. We have run several simulations in such a way that flat dispersion, lower

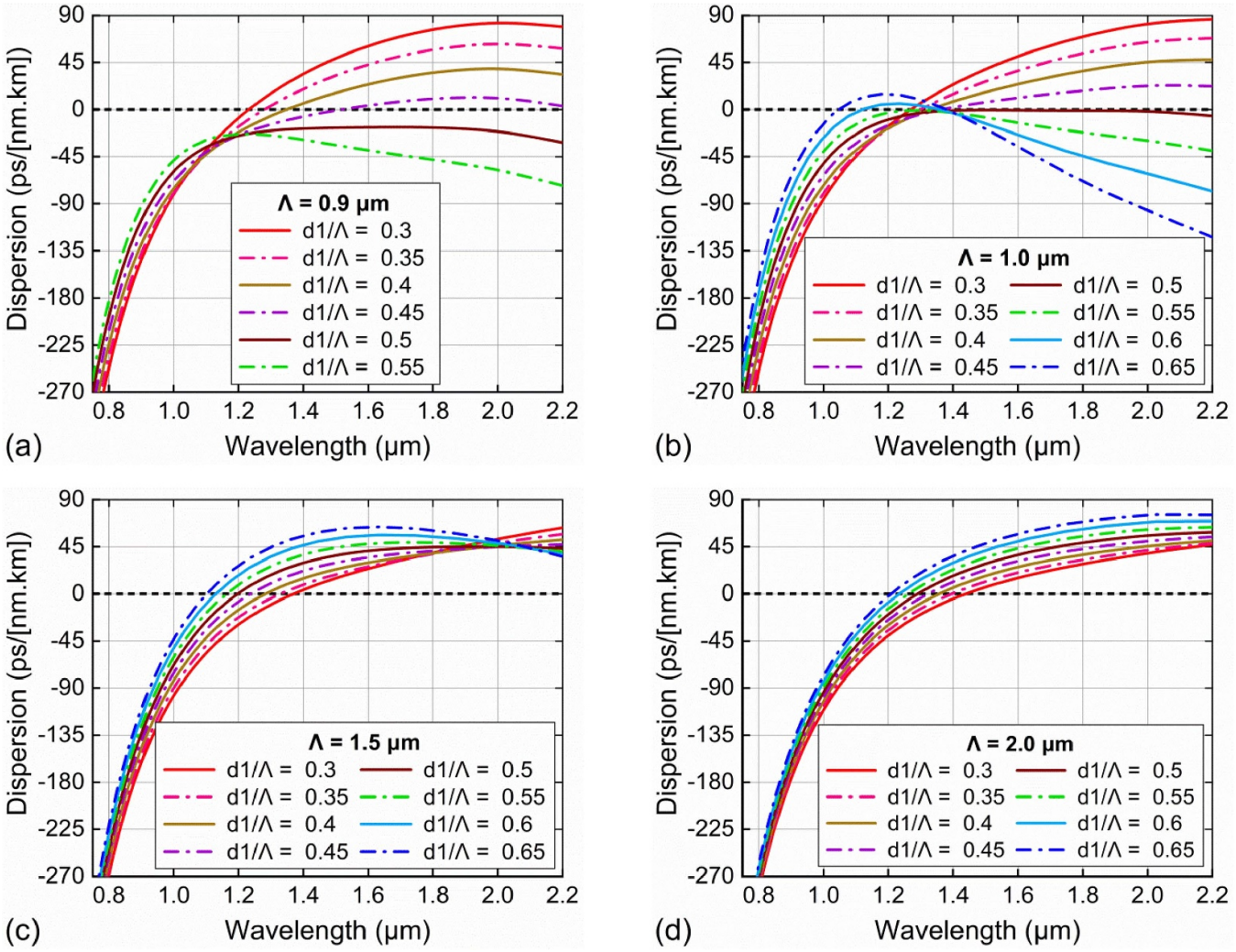

Figure 3. The chromatic dispersion characteristics of C_6H_6-filled circular PCFs with various of d_1/Λ and $\Lambda = 0.9$ μm (a), 1.0 μm (b), 1.5 μm (c) and 2.0 μm (d).

values over a wide wavelength range and suitable ZDWs can be achieved.

Figure 3 displays the dispersion profile of the PCFs for 0.8–2.2 μm wavelength. Initially, $\Lambda = 0.9$ μm, all-normal and anomalous dispersion profiles with a ZDW are explored. The dispersion curves tend to shift below the zero dispersion curve in the wavelength region with $\lambda > 1.1$ μm, implying that all-normal dispersion can be found with increasing d_1/Λ ratio. The two PCFs with $d_1/\Lambda = 0.55$ and 0.5 show all-normal dispersion, in which the dispersion curve with $d_1/\Lambda = 0.5$ is the flattest and the flatness covers a fairly wide wavelength range. Increasing Λ to 1.0 μm, the all-normal dispersion curve $d_1/\Lambda = 0.5$ shifts closer to the zero dispersion curve, becoming ultra-flat dispersion with values as low as ± 0.996 ps nm^{-1} · km spanning from 1.32 μm to 2.06 μm. This is a useful indication for the application of this fiber for broadband and low noise SCG. When $\Lambda = 1.5$ and 2.0 μm, the dispersion curves are all anomalous with one ZDW and the ZDWs shift towards short wavelengths, which can pose challenges in the selection of a suitable pump wavelength. In the case of small-core PCFs ($\Lambda = 0.9$ μm and 1.0 μm), the diversity in dispersion characteristics can be attributed to the competition between material dispersion and waveguide dispersion. For smaller d_1/Λ, material dispersion is more dominant while waveguide dispersion has a stronger influence for larger d_1/Λ. It can be seen that effectively controlling dispersion involves appropriately adjusting the ratio d_1/Λ and Λ is the most convenient way.

For PCFs with small core sizes ($\Lambda = 0.9$ μm and 1.0 μm), the ZDWs shift toward longer wavelengths as d_1/Λ increases. Among the anomalous dispersion profiles, the structure with $d_1/\Lambda = 0.45$ has ZDW = 1.517 μm and is the PCF with the flattest anomalous dispersion, suggesting us to propose this PCF fiber for SCG with a pump wavelength of 1.55 μm. The dependence of ZDWs on structural parameters is presented in figure 4(a). Figure 4(b) also displays the variation of the maximum dispersion value (D_{max}) with the ratio d_1/Λ corresponding to each lattice constant Λ. For $\Lambda = 0.9$ μm, these values decrease with increasing d_1/Λ, in which the structure with $d_1/\Lambda = 0.45$ has D_{max} closest to zero dispersion. When $\Lambda = 1.0$ μm, D_{max} decreases against the increase of d_1/Λ but it increases when d_1/Λ is greater than 0.55. Among them, PCFs

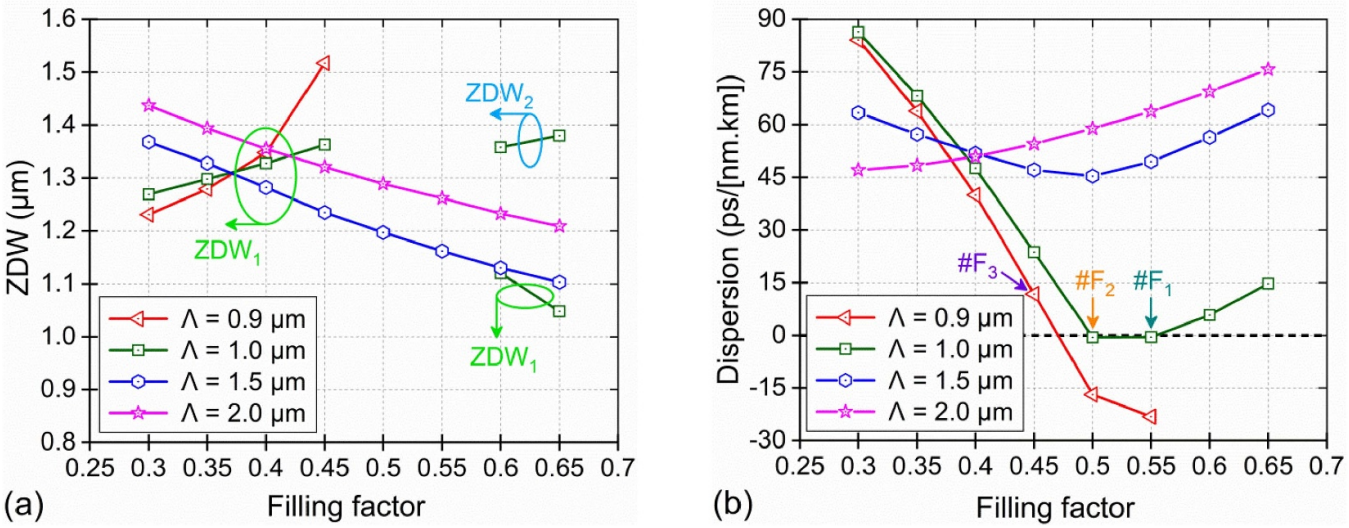

Figure 4. The ZDWs and maximum dispersion values as a function of Λ and d_1/Λ of C_6H_6-filled circular PCFs.

with $d_1/\Lambda = 0.5$ and 0.55 have D_{max} closer to zero. A low dispersion value, near zero is one of the goals of PCF dispersion optimization to apply them to SCG.

It is known that SCG is a complex interactive process involving a series of nonlinear effects and dispersion characteristics play an important role in determining the quality of the SCG spectrum. SPM gives rise to an intensity dependent phase shift that causes a broadened oscillation spectrum at the output [27]. The smooth, highly coherent SCG spectrum results from using fibers with all-normal dispersion or laser pulses excited in the normal dispersion regime. SCG can also be affected by direct generation of new frequency components through higher order nonlinear effects such as Raman scattering, SF, SSFS, DW, etc when pumping PCF in anomalous dispersion regime. We find that three structures with $\Lambda = 1.0$ μm; $d_1/\Lambda = 0.55$, $\Lambda = 1.0$ μm; $d_1/\Lambda = 0.5$, and $\Lambda = 0.9$ μm; $d_1/\Lambda = 0.45$ are the best candidates for efficient SC generation at wavelengths greater than 1.5 μm (figure 5(a)). These PCFs are named $\#F_1$, $\#F_2$, and $\#F_3$ respectively. $\#F_1$ has all-normal dispersion properties with a typical parabolic curve, dispersion value -10.116 ps nm^{-1}·km at pump wavelength of 1.55 μm. $\#F_2$ has ultra-flat dispersion, near-zero with fluctuation of ± 0.996 ps nm^{-1} ·km in the wavelength range 0.74 μm. Its dispersion value of -1.097 ps nm^{-1} ·km at pump wavelength 1.75 μm. These fibers are expected to generate a broad, smooth SCG spectrum. With the air hole design in the innermost ring of the cladding having an elliptical shape and infiltrating $C_6H_5NO_2$ into the hollow core, the publication [44] achieved ultra-flat dispersion but the fluctuation is quite large (about 40 ps nm^{-1} · km). The work [18] also obtained ultra-flat dispersion with a fluctuation of 1 ps nm^{-1} · km over a 5.0 μm wide wavelength region using a PCF filled with C_2H_5OH. The ultra-flat dispersion is expected to increase the ability to broaden the SCG spectrum, achieving the desired bandwidth. This has also been verified in papers [9, 18, 44]. $\#F_3$ possesses the flattest anomalous dispersion among the dispersion curves studied, values as low as 9.315 ps nm^{-1} · km at a pump wavelength of 1.75 μm (ZDW = 1.517 μm). This fiber will emit a broad SCG spectrum under the influence of mechanisms related to soliton dynamics. The ability of PCFs to confine light in the core also depends on the core size. A large core size is more convenient for the manufacturing process, but it is difficult to confine light within it. The core diameter of the three proposed PCFs are 1.34 μm, 1.4 μm, 1.314 μm, respectively (table 2).

The characteristic quantities, including confinement loss (L_c), effective mode area (A_{eff}), and nonlinearity coefficient (γ) of the three proposed fibers, are shown in figures 5(b)–(d). Breaking the periodicity of air holes in the cladding and infiltrating C_6H_6 into the hollow core of the PCFs resulted in effective improvement of the nonlinear properties of the proposed fibers. These PCFs exhibit the low confinement loss in the wavelength region less than 2.0 μm (consistent with the transmission spectrum analysis of C_6H_6 above). $\#F_1$ has the lowest confinement loss, the L_c values at the pump wavelengths of the three fibers are 67.996 dB m^{-1}, 90.197 dB m^{-1}, 97.924 dB m^{-1} respectively. PCFs with larger cores often have poorer light confinement in the core due to leakage of electromagnetic field modes from the core into the cladding or between the air holes through the bridges formed in between them, which increases the value of the effective mode area. $\#F_2$ has the largest A_{eff}, which is 2.982 μm^2, at a pumping wavelength of 1.75 μm. The A_{eff} values of the three PCFs at different wavelengths are 2.466 μm^2, 2.982 μm^2, 2.868 μm^2, respectively. On the contrary, the nonlinear coefficient of $\#F_1$ is the highest, because γ is always inversely proportional to A_{eff}. We have achieved values of γ as high as several 1000 W^{-1} · km^{-1}, higher than some previous publications on PCFs infiltrated to various fluids [16, 17, 20, 33]. The structural parameters and values of the characteristic quantities of the three proposed fibers, are presented in table 2.

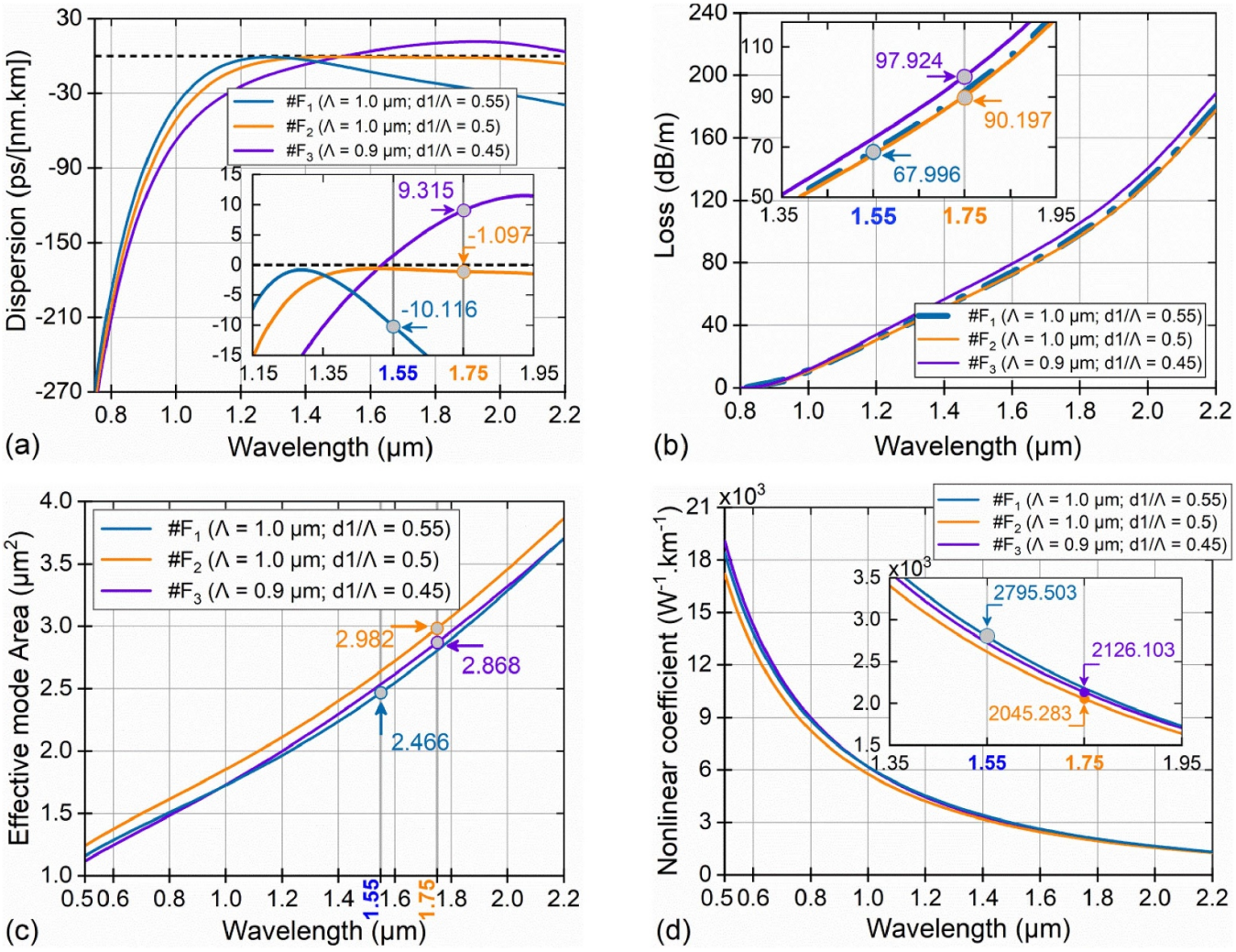

Figure 5. The characteristic quantities including dispersion, confinement loss, effective mode area, and nonlinearity coefficient of the three proposed PCFs.

Table 2. The structure parameters and the characteristic quantities of proposed PCFs at the pump wavelength.

#	D_c (μm)	Λ (μm)	d_1/Λ	Pump wavelength (μm)	A_{eff} (μm^2)	$\gamma(W^{-1}\cdot km^{-1})$	D (ps nm$^{-1}\cdot$ km)	L_c (dB m^{-1})
$\#F_1$	1.34	1.0	0.55	1.55	2.466	2795.503	–10.116	67.996
$\#F_2$	1.4	1.0	0.5	1.75	2.982	2045.283	–1.097	90.197
$\#F_3$	1.314	0.9	0.45	1.75	2.868	2126.103	9.315	97.924

4. Supercontinuum generation in near and mid-infrared range

In section 3, the dispersion properties including profile, flatness, and value of PCFs were analyzed based on the corresponding graphs against wavelength, from which three optimal PCFs were proposed for SCG. The characteristic quantities, i.e. loss, effective mode area, and nonlinear parameters are also discussed in detail. We use these PCFs to analyze the temporal and spectral behavior of the optical pulses in each fiber length. So, the following topics are entirely concerned with supercontinuum generation in optimally PCFs.

One question is whether the proposed PCF with suitable dispersion and high nonlinearity can generate new frequency components at the fiber end. Thus, the evolution of the optical pulse, whose slowly varying electric field amplitude is represented by the envelope function $A(z, T)$, propagating along the fiber is described by solving the generalized nonlinear Schrödinger equation symmetry split-step Fourier transform method [11, 27].

$$\frac{\partial A(z,T)}{\partial z}+\frac{\alpha}{2}A(z,T)-\sum_{n\geqslant 2}\frac{i^{n+1}}{n!}\beta_n\frac{\partial^n A(z,T)}{\partial T^n}$$
$$=i\gamma\left(1+\frac{i}{\omega_0}\frac{\partial}{\partial T}\right)\left[A(z,T)\int_{-\infty}^{\infty}R(T')\left|A(z,T-T')\right|^2 dT'\right]. \quad (6)$$

Table 3. The coefficient of higher-order dispersion at the pump wavelength.

Coefficient	#F_1_All-normall 1.0/0.5	#F_2_All-normall 1.0/0.55	#F_3_Anomalous 0.9/0.45
β_2 (ps^2 m^{-1})	1.292×10^{-02}	1.747×10^{-03}	-1.506×10^{-02}
β_3 (ps^3 m^{-1})	-1.072×10^{-04}	-5.414×10^{-06}	9.186×10^{-05}
β_4 (ps^4 m^{-1})	5.408×10^{-07}	-1.770×10^{-07}	1.489×10^{-07}
β_5 (ps^5 m^{-1})	1.119×10^{-10}	9.903×10^{-10}	-2.770×10^{-09}
β_6 (ps^6 m^{-1})	-2.544×10^{-11}	1.048×10^{-10}	-7.850×10^{-12}
β_7 (ps^7 m^{-1})	4.176×10^{-14}	-2.721×10^{-12}	1.018×10^{-13}
β_8 (ps^8 m^{-1})	9.036×10^{-15}	1.710×10^{-14}	8.047×10^{-15}
β_9 (ps^9 m^{-1})	-1.566×10^{-16}	6.096×10^{-16}	-1.610×10^{-16}
β_{10} (ps^{10} m^{-1})	-3.084×10^{-19}	-1.740×10^{-17}	1.082×10^{-18}
β_{11} (ps^{11} m^{-1})	4.451×10^{-20}	1.637×10^{-19}	-7.894×10^{-21}

The model includes linear effects (dispersion and loss—depicted on the left-hand side of the equation) and nonlinearity (on the right—hand side). In this equation, α and β are loss and dispersion in the frequency domain, respectively, extracted from the data of figures 5(a)–(d). The higher order dispersion (even up to sixth order) has a significant influence on spectral broadening when analyzing and processing very broad SCG spectra. Therefore, they are calculated through the development coefficient of the Taylor series at the pumping pulse frequency ω_0 (equations (7) and (8)) [27].

$$\beta(\omega) = \beta(\omega_0) + \beta_1(\omega_0)(\omega - \omega_0) + \frac{1}{2!}\beta_2(\omega_0)(\omega - \omega_0)^2 + \ldots. \quad (7)$$

The nth order dispersion is related to the derivative of the phase constant β with respect to the angular frequency ω, which is determined by [27]. Table 3 displays the higher-order dispersion at pump wavelength in our numerical model.

$$\beta_n = \frac{\mathrm{d}^n\beta}{\mathrm{d}\omega^n}|_{\omega=\omega_0} \quad (8)$$

However, the higher order (up to eleventh order) dispersion values in our simulations are so small that they may have a negligible impact on the SCG spectral broadening if short pulses of less than ten picoseconds are used. The energy transfer from the fundamental mode to the higher order mode can be prevented because the walk-off between the two modes is large enough [49]. Therefore, our subsequent analysis of the evolution of SCG is mainly devoted to the fundamental mode.

In our model, the laser pulses are modeled by Gaussian pulses centered at the pump wavelength and expressed as in equation (9).

$$A(z,T) = \sqrt{P}\exp\left(-\frac{T^2}{2T_0^2}\right), \quad (9)$$

where P and T_0 respectively represents the peak power and duration of input pulse at the reference frequency ω_0. In equation (6), $R(T')$ is the Raman response function, the sum of all contributing mechanisms listed by Zhao *et al* [36], which depends mainly on the nonlinear optical response of C_6H_6 due to the combination of bound-electronic and nuclear contributions. Compared to the pulse duration, the electron-bound nonlinearity mechanism responds to the impact of external field in a very short time, making it an instantaneous mechanism [13].

The picosecond (high average power) laser sources have the potential to generate SCGs in the visible and near-infrared regions due to their high power density while the femtosecond lasers are supreme sources for generating coherent SCGs in the visible, near-infrared or mid-infrared regions [50]. The dispersion regimes and nonlinear characteristics of the fiber in addition to pulse duration and pump power govern the stability of the acquired SCG spectrum. Further, the input pulse can be maximally compressed in the time domain simultaneously broaden SCG in the frequency domain if an appropriate fiber length is chosen. In the next section, the properties of the SCG are simulated based on the proposed PCFs with all-normal and anomalous dispersion regimes, using femtosecond laser pulse.

4.1. SCG with all-normal dispersion PCFs

For #F_1: It has an all-normal dispersion, with a typical parabolic profile and quite low dispersion -10.116 ps nm^{-1}·km at a pump wavelength of 1.55 μm. The small effective mode area of 2.466 μm^2 and low confinement loss of 67.996 dB m^{-1} will provide many advantages for broadening the SCG spectrum with typical characteristics associated with non-soliton dynamic mechanisms. Moreover, the benefit of all-normal dispersion in creating SCG is for a flatter, smoother spectrum. In the simulation, a laser source having wavelength 1.55 μm is utilized as the pump for the simulation purposes. Pulses of 40 fs duration with various input energies (E) of 0.006, 0.008, and 0.01 nJ (corresponding peak power (P) of 150, 200, and 250 W), propagates in 5.5 cm PCF length, giving SCG spectra with different widths exposed in figures 6(a), (c), (f) and (i). The bandwidth increases with the peak power of the input pulse, the SCG spectrum shows a smooth profile with very small fluctuations in the short wavelength region because the newly generated spectral components in the flat top region will not undergo the fluctuations are clearly dispersed. With $P = 250$ W, the SCG spectrum is the widest, spanning from 0.803 to 2.13 μm, corresponding to a bandwidth at 30 dB of 1.215 μm (figure 6(b)).

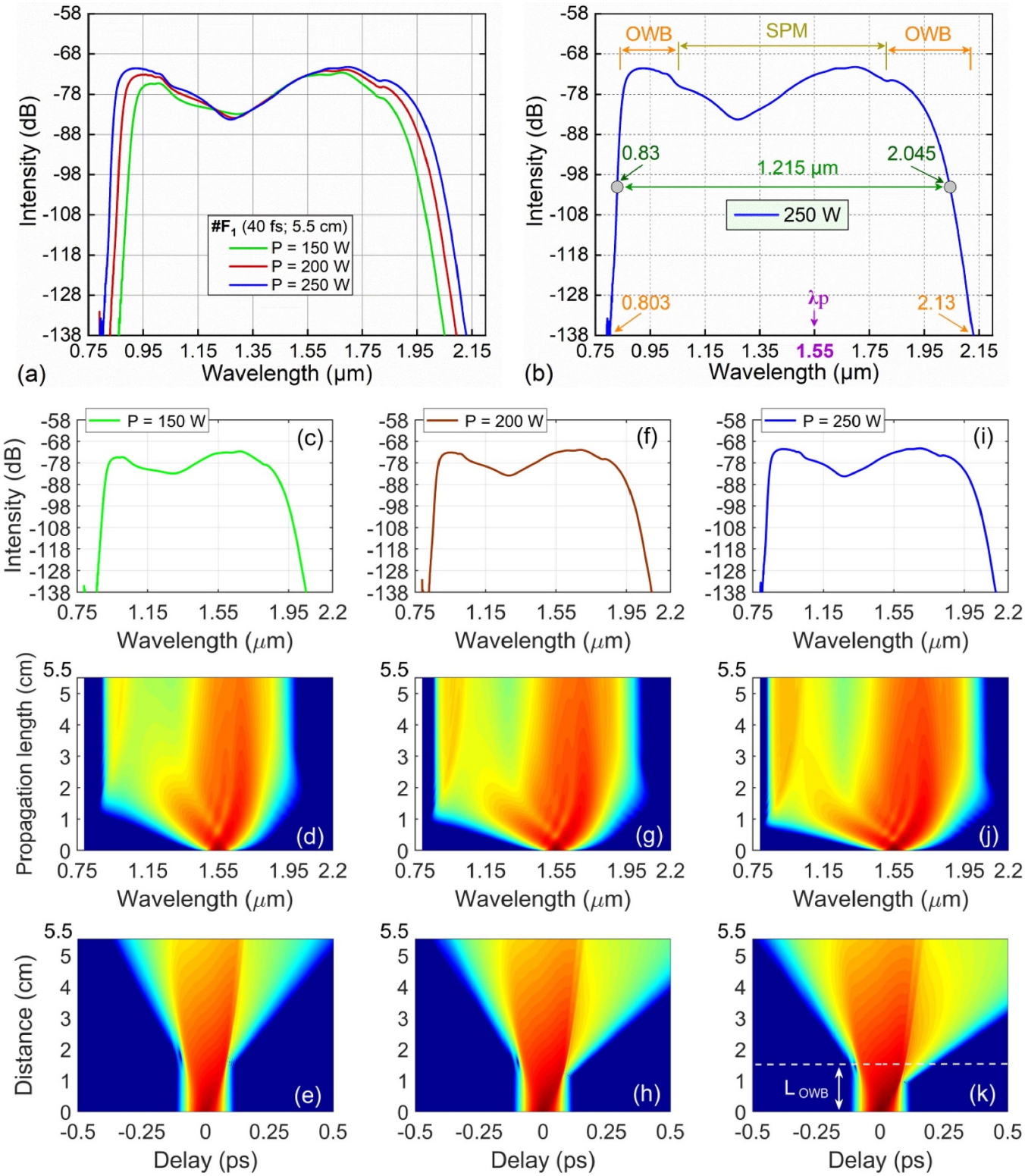

Figure 6. For #F_1 fiber (length of 5.5 cm): the output spectrum for various input pulse energies when using pump pulses with 1.55 μm pump wavelength and 40 fs duration (a), the output spectrum with the input pulse peak power of 250 W (b), the temporal profile at various propagation length (d), (g), (j) and the pulse evolution of the SC along the fiber (e), (h), (k).

The temporal profile at various propagation lengths and the pulse evolution of the SC along the fiber are shown in figures 6(d), (e), (g), (h), (j) and (k). The broadening of SCG to the near-infrared region is achieved through the SPM and OWB mechanisms. Due to the deterministic nature of the SPM and OWB effects, the SCG spectrum, acquired at each step of the propagation length, has a high degree of coherence over the entire spectral range. The asymmetric spectral broadening

is attributed to the SPM nonlinear effect followed by OWB and dispersion effects. OWB appears early on the blue edge even at SCG with a low power of only 150 W. In the case of $P = 250$ W, the pulse undergoes OWB, which occurs at the leading and trailing edges of the pulse after propagating short distances, more than a centimeter. New frequency components are created through the overlap of different pulse spectrum components due to OWB associated with FWM. Furthermore, the slower short-wavelength propagation speed at the trailing edge compared to the pulse tail at the center of the pulse is responsible for the appearance of OWB due to the temporary overlap between the pulse tail and the trailing edge. The sinusoidal beating between them clearly demonstrates this phenomenon [51] (figure 6(j)). The first observed OWB distance (L_{OWB}) of 1.621 cm is calculated from the formula: $L_{\mathrm{OWB}} = \frac{T_0^2}{\beta_2}\sqrt{\frac{3\beta_2}{2\beta_2+2\gamma P_0 T_0^2}}$. This value also matches the position representing the start of the OWB process (dashed line in figure 6(k)). The pulse spectrum then continues to expand toward blue-side and red-side, the newly created spectral wavelengths will be energized from the central part of the pulse spectrum. In the longer wavelength region, the large value of the effective mode area and the low nonlinear coefficient cause the spectrum to extend only to the near infrared region (2.13 μm). The achieved broad SCG spectrum covers the near-infrared region and extends from 0.803 μm to 2.13 μm, a spectral width of 1.215 μm at 30 dB level, along with a smooth spectral profile.

For #F_2: #F_2 has a flatter dispersion profile in comparison to #F_1. It has near-zero and ultra-flat dispersion, with $\Delta D = \pm 0.996$ ps nm^{-1}·km over a wavelength range as wide as 0.74 μm. Moreover, at the pump wavelength of 1.75 μm, its dispersion value -1.097 ps nm^{-1}·km is much smaller than #F_1. These outstanding feature allows to expect that the SCG spectrum based on #F_2 will be much more broadened than that of #F_1, the result is illustrated in figures 7(a)–(c), (f) and (i). A laser pulse of 40 fs duration, pumped at 1.75 μm, propagates in a 5.5 cm length fiber #F_2. The SCG spectrum was investigated with changes in input energy $E = 0.006$, 0.008, 0.01 nJ, corresponding to peak power $P = 150$, 200, 250 W. The influence of input peak power on the spectra and pulse width is shown in figure 7(a). Similar to the SCG process for #F_1, the optical spectrum is obviously broadened by the enhanced SPM effect as the peak power of the pump pulse increases. The bandwidth increases gradually, the spectrum is smooth and some small fluctuations appear, especially with the peak power of 250 W. This is also a typical characteristic of the SCG spectrum when pumping PCFs in normal dispersion regime. We obtained a maximum bandwidth of 1.626 μm at 30 dB with $P = 250$ W (equal to the peak power in the case of #F_1). The spectrum spans to the near-infrared region from 0.858 to 2.6 μm. Although #F_2 has a larger effective mode area, lower nonlinear coefficient, and higher confinement loss than #F_1, the spectral bandwidth at 30 dB is much larger, about 1.34 times. This is attributed to the near-zero ultra-flat dispersion with its small fluctuations over a wide wavelength range.

Figures 7(d), (e), (g), (h), (j) and (k) show the spectral and temporal profile of the SCG generated at the output of 5.5 cm long #F_2. The spectrum is asymmetrically broadened due to the SPM and OWB effects, even with input energy as low as 0.006 nJ (the peak power of 150 W). In the case of 250 W, the bandwidth of the SCG slightly broadens toward the shorter wavelength side, OWB first appears at a propagation distance of about 5 cm (dashed line in figure 7(k)), corresponding to the calculated value is 5.178 cm. In addition, the increasing propagation loss and high dispersion slope also limit the expansion of the SCG towards both sides of the spectrum. To further illustrate the influence of nonlinear effects on the SCG spectral characteristics of fibers #F_1 and #F_2 with a peak power of 250 W, the characteristic length includes the nonlinear length ($L_{\mathrm{NL}} = \frac{1}{\gamma P}$), dispersion length, ($L_{\mathrm{D}} = \frac{T_0^2}{|\beta_2|}$) and L_{OWB} is computed and presented in table 4. It can be seen that, L_{D} is much larger than L_{NL}, so the behavior of light in PCF comes from a nonlinear mechanism and the broadened spectrum is due to the interaction between all-normal dispersion and SPM [52].

4.2. SCG with anomalous dispersion PCF

The ways in which anomalous dispersion affects SCG quality (figure 8) will be discussed in the next section, nonlinear effects related to soliton dynamics such as SF, SRS, SSFS, and DW,… are the main mechanisms explaining the spectral properties. The broad but noisy spectrums are obtained when #F_3 is pumped at 1.75 μm wavelength near ZDW (1.517 μm). The laser pulses with input energies of 0.018, 0.022, and 0.026 nJ (corresponding to $P = 90$, 110, and 130 W, respectively) and duration of 200 fs travel through 20 cm of fiber length. Figures 8(a)–(c), (f) and (i) evinces that the SCG bandwidth gradually increases with increasing peak power, but the difference is not significant. With a peak power ($P = 130$ W), the SCG spectrum spans into the mid-infrared region (red-side extended to 3.868 μm), a maximum bandwidth of 2.467 μm at 30 dB is found (figure 8(b)). It has been confirmed that the soliton pulse propagation is obtained by balancing the SPM and anomalous dispersion of fiber. This fundamental soliton propagates along the fiber without any changes, both in temporal and spectral shape. However, the above balance is broken and both the temporal and spectral shape of the soliton undergo complex changes (figures 8(d), (e), (g), (h), (j) and (k)) due to the appearance of higher order soliton (the shape of higher order soliton changes periodically) with higher power propagate along the fiber. Under the influence of pulsed Raman scattering and high-order dispersion, the higher order solitons are divided into a series of elementary solitons [53, 54]. This phenomenon is soliton fission, which is mainly responsible for the continuous broadening of the output pulse even with input pulse peak powers as low as 90 W.

Considering the SCG formation process with $P = 130$ W, we find that the SCG spectrum is narrow and symmetric due to the main influence of the SPM effect in the first few centimeters of the propagation process. Then, SF begins to play a role at a propagation length of about 6 cm as the input pulse approaches the ZDW. The red shift is due to the formation

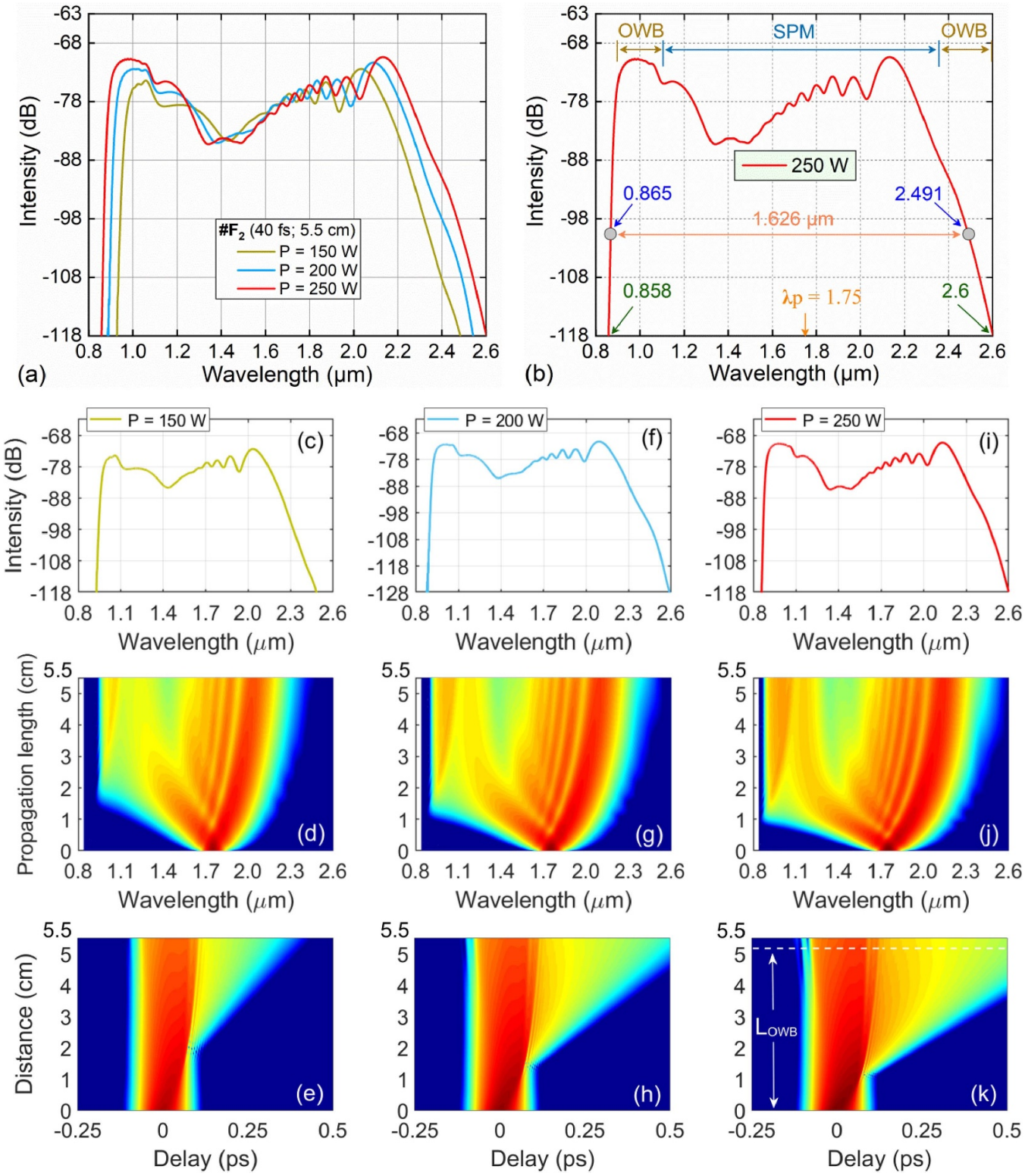

Figure 7. For #F_2 fiber (length of 5.5 cm): the output spectrum for various input pulse energies when using pump pulses with 1.75 μm pump wavelength and 40 fs duration (a), the output spectrum with the input pulse peak power of 250 W (b), the temporal profile at various propagation length (d), (g), (j) and the pulse evolution of the SC along the fiber (e), (h), (k).

of first-order solitons, as a highest energy and shortest duration soliton, with different central wavelengths moving to the longer wavelength region, known as the SSFS effect. The long wavelength of the continuous band is up to 3.868 μm in the near infrared region. Once SF occurs, the remaining energy after break-up is dissipated as a DW [55], causing a blue shift in the spectrum, thus developing a broader spectrum toward the short wavelengths of 0.842 μm. But unfortunately, in the

Table 4. The various length distribution of SCG in $\#F_1$ and $\#F_2$ for 250 W peak power.

#	E (nJ)	T_0 (fs)	P (W)	β_2 (ps^2 m^{-1})	γ(W^{-1} · km^{-1})	L_D (cm)	L_{NL} (cm)	L_{OWB} (cm)
$\#F_1$	0.01	40	250	1.292×10^{-2}	2795.503	12.4	0.143	1.621
$\#F_2$	0.01	40	250	1.747×10^{-2}	2045.283	91.6	0.196	5.178

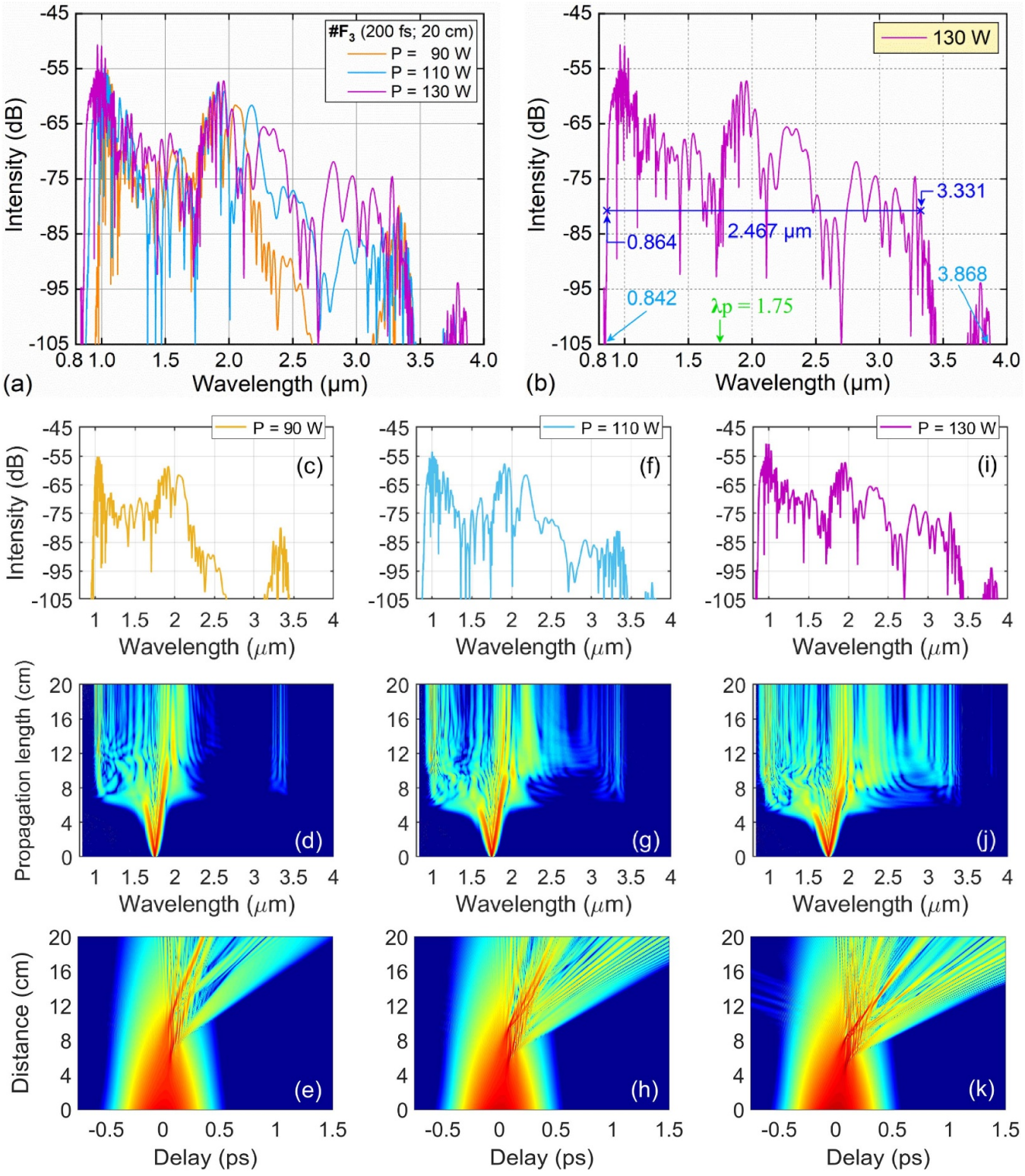

Figure 8. For $\#F_3$ fiber (length of 20 cm): the output spectrum for various input pulse energies when using pump pulses with 1.75 μm pump wavelength and 200 fs duration (a), the output spectrum with the input pulse peak power of 130 W (b), the temporal profile at various propagation length (d), (g), (j) and the pulse evolution of the SC along the fiber (e), (h), (k).

Table 5. Contrast of soliton order and various length distribution of SC generation in $\#F_3$ for 130 W peak power.

#	E (nJ)	T_0 (fs)	P (W)	β_2 (ps^2 m^{-1})	γ(W^{-1} · km^{-1})	L_D (cm)	L_{NL} (cm)	N	L_{fiss} (cm)
$\#F_3$	0.026	200	130	-1.506×10^{-2}	2126.103	265.7	0.362	27.092	9.807

shorter wavelength region the speed of the blue-shifted DWs when they catch up with the first ejected soliton due to the high dispersion slope is reduced, which limits the spectral broadening towards the blue-side. Similarly, in the longer wavelength region, the large effective mode area leads to low nonlinear coefficients also reducing redshift. SCG spectrum with maximum width of 2.467 μm at 30 dB is achieved.

The influence of soliton dynamics on the continuous expansion of the output pulse is further verified by calculating characteristic lengths such as SF length ($L_{fiss} = \frac{L_D}{N}$), soliton order ($N^2 = \frac{L_D}{L_{NL}}$). These values include both L_{NL} and L_D are illustrated in table 5. Obviously, L_{NL} is too small compared to L_D and L_{PCF} (PCF length), so soliton dynamics with typical nonlinear effects dominate here. In addition, the very small value of the second order dispersion β_2 and the extremely large value of L_D of 265.7 cm (much larger than the fiber length of 20 cm) further emphasize the doinance of the SF effect.

5. Conclusion

The breaking of the periodicity of the air holes in the cladding, cleverly combined with the high nonlinearity of the core region (due to the infiltration C_6H_6 into the core), has brought advantages in optimizing the dispersion properties of PCFs. The flat all-normal and anomalous dispersions (especially the ultra-flat dispersion with low fluctuations $\pm$0.996 ps nm^{-1}·km in the 0.74 μm wavelength region) verified the ability to transmit broadband SCG with very low peak power In the near-infrared and mid-infrared regions of PCFs using silica glass. It can be seen that our designed PCF is at a good level in terms of exhibiting valuable optical properties, potential in fiber fabrication, and low peak power for SCG-related applications. At 250 W peak power, two PCFs ($\#F_1$ and $\#F_2$) with all-normal dispersion showed outstanding advantages in the SCG process. By pumping them at wavelengths of 1.55 and 1.75 μm with pulses of the same duration of 40 fs, the SCG spectral widths are 1.327 μm and 1.742 μm (corresponding to bandwidths at 30 dB of 1.215 μm and 1.626 μm, respectively). Although it does not have the advantages of characteristic quantities (the larger effective mode area, lower nonlinear coefficient, and higher attenuation), $\#F_2$ still demonstrates the ability to emit SCG with a spectral width of 30 dB is much greater than $\#F_1$. This further proves that the ultra-flat, near-zero dispersion is very valuable in broadening the spectrum, helping to improve SCG performance. To the best of our knowledge, the 1.742 μm spectral width (1.626 μm spectral width at 30 dB) of $\#F_2$ is the largest despite the lowest peak power among previous publications for benzene-core silica glass-based PCFs or even with PCF infiltrated in into other nonlinear fluids. The comparisons between the SCG spectra width and peak power of our novel-designed PCFs with other studies are displayed in table 6. The flat anomalous dispersion, effective mode area is quite small 2.868 μm^2 (highly nonlinear coefficient of 2126.103 W^{-1} · km^{-1}) and loss as low as 97.924 dB m^{-1} are favorable conditions for $\#F_3$, pumped in anomalous dispersion regime, to enable SCG with a spectral width of up to 3.026 μm corresponding to a bandwidth of 2.467 μm at the 30 dB with very low peak power, as low as 130 W. Table 6 also shows that this fiber has a similar large spectral width [38] but a peak power about 4.1 times lower. Although its spectral width is 0.9 times that of [39], the peak power is 6.08 times lower. As for PCFs with other anomalous dispersions, SCG with this fiber both provides a larger bandwidth and uses much lower peak power. Within the scope of research on liquid-core silica glass-based PCFs, the proposed PCF projects yield promising results for various SCG-related applications in the near and mid-infrared regions. Broadband SCG sources with low peak power can be effective alternatives to traditional glass SCG sources.

Table 6. The spectral width and peak power of the proposed PCFs in comparison with other studies on liquid infiltrated PCF.

Structures	Liquids	Fiber length (cm)	Pump wavelength (μm)	Dispersion regime	SC range (μm)	Input peak power (W)	References
#F_1 Circular	C_6H_6	5.5	1.55	all-normal	1.327	250	This work
#F_2 Circular		5.5	1.75	all-normal	1.742	250	
#F_3 Circular		20	1.75	anomalous	3.026	130	
#F_1 Hexagonal	C_6H_6	1	1.56	all-normal	1.3	55 000	[32]
#F_2 Hexagonal		1	1.56	anomalous	2.0	11 100	
#F_3 Hexagonal		1	1.56	anomalous	2.9	22 200	
#CBF_1 Circular	C_6H_6	1.0	1.064	all-normal	0.87	450	[13]
#SBF_2 Square		1.0	1.3	all-normal	1.050	450	
#HBF_3 Hexagonal		1.0	1.3	all-normal	1.11	450	
#F_1 Square	C_6H_6	1.0	1.3	all-normal	1.04	450	[38]
#F_2 Square		15	1.55	anomalous	3.15	537	
#F_1 Circular	C_6H_6	1	1.3	all-normal	1.1	450	[39]
#F_2 Circular		12	1.5	anomalous	3.4	790	
#F_1 Circular	C_7H_8	10	1.55	anomalous	2.0	556	[9]
#F_2 Circular		1	1.55	all-normal	1.3	375	
#I_0.3 Hexagonal	C_7H_8	10	1.55	all-normal	0.575	7140	[16]
#I_0.35 Hexagonal		10	1.55	anomalous	0.75	6670	
Hexagonal	C_2H_5OH	20	1.55	anomalous	1.0	50 000	[18]
#F_1 Square	CS_2	10	1.3	all-normal	0.878	18 750	[22]
PCF with elliptical air-holes	$C_6H_5NO_2$	5	1.81	anomalous	1.5	1000	[44]
#F_1 Hexagonal	CCl_4	30	1.35	anomalous	1.3	2670	[56]
#F_2 Hexagonal		30	1.064	all-normal	0.35	2670	
#F_1 Hexagonal	C_2Cl_4	5	1.56	all-normal	1.18	16 670	[33]
#F_2 Hexagonal		10	1.56	anomalous	1.0	16 670	
#F_3 Hexagonal		10	1.03	anomalous	1.7	20 830	
#F_1 Square	$CHCl_3$	10	0.95	all-normal	0.732	1440	[20]
#F_2 Square		10	1.4	anomalous	2.36	20 000	
Hexagonal	$CHCl_3$	1	1.06	anomalous	1.020	47 000	[57]

Acknowledgments

This work was supported by Hue University under the Core Research Program, Grant Nos. NCTB.DHH.2024.07.

References

[1] Baljinder K, Santosh K and Brajesh K K 2022 *Opt. Fiber Technol.* **72** 102982
[2] Khan K R, Mahmood M F, Biswas A and Belic M 2016 *J. Nanoelectron. Optoelectron.* **11** 497–505
[3] Chen C, Shi W, Reyes R and Yang V X 2018 *Biomed. Opt. Express* **9** 6529–44
[4] Poudel C and Kaminski C F 2019 *J. Opt. Soc. Am.* B **36** A139–53
[5] Thi T N, Trong D H and Van L C 2024 *Opt. Quantum Electron.* **56** 367
[6] Jain S K, Sharma R, Amrit P, Chandna V K, Sharma G, Yadav A K and Vyas S 2023 *Mater. Today* **74** 255–8
[7] Zhang H P, Zhao B, Ma R Z, Li Z R and Wang P F 2023 *Laser Phys.* **33** 125401
[8] Thi T N, Trong D H and Van L C 2023 *Laser Phys.* **33** 055102
[9] Thi T N, Trong D H and Van L C 2023 *Opt. Quantum Electron.* **55** 93
[10] Alam M Z, Tahmid M I, Mouna S T, Islam M A and Alam M S 2021 *Opt. Commun.* **500** 127322
[11] Dudley J M and Taylor J R 2010 *Supercontinuum Generation in Optical Fibers* (Cambridge University Press) (https://doi.org/10.1017/CBO9780511750465)
[12] Ferhat M L, Cherbi L and Haddouche I 2018 *Optik* **152** 106–15
[13] Van L C, Tran B T L, Thi T N, Trong D H, Van T D, Mai T D, Ngoc H T, Doan T T and Quoc K D 2022 *Opt. Quantum Electron.* **54** 840
[14] Begum F and Abas P E 2019 *Prog. Electromagn. Res.* C **89** 149–59

[15] Li J, Wang J, Teng Y, Xu Z and Cheng J 2020 *Opt. Quantum Electron.* **52** 447
[16] Van L C, Anuszkiewicz A, Ramaniuk A, Kasztelanic R, Xuan K D, Long V C, Trippenbach M and Buczyński R 2017 *J. Opt.* **19** 125604
[17] Hoang V T, Kasztelanic R, Stępniewski G, Xuan K D, Long V C, Trippenbach M, Klimczak M, Buczyński R and Pniewski J 2020 *Appl. Opt.* **59** 3720–5
[18] Le H V, Cao V L, Nguyen H T, Nguyen A M, Buczyński R and Kasztelanic R 2018 *Laser Phys.* **28** 115106
[19] Thi T N and Van L C 2023 *J. Opt.* **52** 2296–305
[20] Thi T N and Van L C 2024 *Mod. Phys. Lett.* B **38** 2350233
[21] Van L C, Hoang V T, Long V C, Borzycki K, Xuan K D, Quoc V T, Trippenbach M, Buczyński R and Pniewski J 2020 *Laser Phys.* **30** 035105
[22] Minh N V T, Van L C, Hong P N T, Hoang V T, Nguyen H T and Le H V 2023 *Optik* **286** 171049
[23] Thi T N, Trong D H, Tran B T L, Van T D and Van L C 2022 *J. Opt.* **51** 678–88
[24] Scheibinger R, Lüpken N M, Chemnitz M, Schaarschmidt K, Kobelke J, Fallnich C and Schmidt M A 2021 *Sci. Rep.* **11** 5270
[25] Hartung A, Bierlich J, Lorenz A, Kobelke J and Jäger M 2019 *J. Opt. Soc. Am.* B **36** 3404–10
[26] Forestier X *et al* 2020 *Appl. Nanosci.* **10** 1997–2005
[27] Agrawal G 2019 *Nonlinear Fiber Optical* 6th edn (Academic) (https://doi.org/10.1016/C2018-0-01168-8)
[28] Engelsholm R D and Bang O 2019 *Opt. Express* **27** 10320–31
[29] Eslami Z, Ryczkowski P, Salmela L and Genty G 2020 *Opt. Lett.* **45** 3103–6
[30] Hoang V T *et al* 2018 *Opt. Mater. Express* **8** 3568–82
[31] Fanjoux G, Margueron S, Beugnot J C and Sylvestre T 2017 *J. Opt. Soc. Am.* B **34** 1677–83
[32] Van L C, Hoang V T, Long V C, Borzycki K, Xuan K D, Quoc V T, Trippenbach M, Buczynski R and Pniewski J 2021 *Opt. Eng.* **60** 116109
[33] Le H V, Hoang V T, Nguyen H T, Long V C, Buczynski R and Kasztelanic R 2021 *Opt. Quantum Electron.* **53** 187
[34] Vyas S, Sharma G, Jain S K, Zafar R and Nayyar A 2023 *Proc. 4th Int. Conf. on Computing, Communications, and Cyber-Security* vol 664 pp 95–104
[35] Thi T N and Van L C 2023 *J. Comput. Electron.* **22** 1507–21
[36] Zhao P, Reichert M, Benis S, Hagan D J and Stryland E W V 2018 *Optica* **5** 583–94
[37] Myers T L, Tonkyn R G, Danby T O, Taubman M S, Bernacki B E, Birnbaum J C, Sharpe S W and Johnson T J 2018 *Appl. Spectrosc.* **72** 535–50
[38] Tran B T L and Van L C 2023 *Eur. Phys. J.* D **77** 90
[39] Tran B T L and Van L C 2023 *Int. J. Modern Phys.* B 2450353
[40] Medjouri A, Simohamed L M, Ziane O, Boudrioua A and Becer Z 2015 *Photonics Nanostruct: Fundam. Appl.* **16** 43–50
[41] Ahmad R, Komanec M and Zvanovec S 2020 *J. Nanophotonics* **14** 026016
[42] Dashtban Z, Salehi M R and Abiri E 2021 *Photonics Nanostruct: Fundam. Appl.* **46** 100942
[43] Saitoh K, Florous N J and Koshiba M 2006 *Opt. Lett.* **31** 26–28
[44] Wen J, Liang B, Qin W, Sun W and Cand Xiong K H 2022 *Opt. Quantum Electron.* **54** 817
[45] Lumerical Mode Solutions, Inc (available at: https://www.lumerical.com/)
[46] Malitson I H 1965 *J. Opt. Soc. Am.* **55** 1205–9
[47] Moutzouris K, Papamichael M, Betsis S C, Stavrakas I, Hloupis G and Triantis D 2013 *Appl. Phys.* B **116** 617–22
[48] Zhu Z and Brown T G 2002 *Opt. Mater. Express* **10** 853–64
[49] Lee Y S, Lee C G, Bahloul F, Kim S and Oh K 2019 *J. Light. Technol.* **37** 1254–63
[50] Krishna G D, Pillai V P M and Gopchandran K G 2020 *Opt. Fiber Technol.* **56** 102198
[51] Finot C, Kibler B, Provost L and Wabnitz S 2008 *J. Opt. Soc. Am.* B **25** 1938–48
[52] Medjouri A and Abed D 2021 *Opt. Quantum Electron.* **53** 399
[53] Chuan P, Kumar A and Kalra Y 2019 *Optik* **187** 230–7
[54] Medjouri A and Abed D 2020 *Optik* **219** 165178
[55] Salimullah S M and Faisal M 2023 *Alex. Eng. J.* **70** 289–300
[56] Dinh Q H, Pniewski J, Van H L, Ramaniuk A, Long V C, Borzycki K, Xuan K D, Klimczak M and Buczyński R 2018 *Appl. Opt.* **57** 3738–46
[57] Wang C C, Li W M, Li N and Wang W Q 2017 *Opt. Laser Technol.* **88** 215